Chemical Engineering Journal 151 (2009) 79–88

Contents lists available at ScienceDirect

Chemical Engineering Journal

journal homepage: www.elsevier.com/locate/cej

Mass transfer from oscillating bubbles in bubble column reactors

Mariano Martín*, Francisco J. Montes, Miguel A. Galán

Departamento de Ingeniería Química y Textil, Universidad de Salamanca, Pza. de los Caídos 1-5, 37008 Salamanca, Spain

ARTICLE INFO

Article history:
Received 29 October 2008
Received in revised form 27 January 2009
Accepted 29 January 2009

Keywords:
Population balance
Mass transfer
Bubble columns
Inviscid fluids
Mathematical modelling
Oscillating bubbles

ABSTRACT

In spite of the amount of work on bubble columns, their design and scale up is still a difficult task due to the lack of understanding of the mass transfer mechanisms. In this work we have studied the contribution of bubble deformation to the mass transfer rate for the air–water system from a theoretical point of view. The specific contact area is obtained using a population balance model. A new scheme for bubble classes has been implemented to account for the effect of bubble oscillations in mass transfer due to coalescence and break-up processes. Meanwhile, a theoretical model for the Sherwood number for oscillating bubbles in inviscid fluids has been used to implement the effect of bubble deformation on the liquid-film resistance. Coupling the population balance with the Sherwood number for oscillation bubbles, k_La values are predicted. It was found that bubble oscillations explain the wide range of parameters often used to fit k_L and the fact that in bubble columns the concentration profiles surrounding individual bubbles are not completely developed due to the presence of other bubbles, in agreement with previous results from the literature.

1. Introduction

Bubble column reactors (BCR's) are widely used in the chemical and biochemical industries because of the advantages they offer such as the lack in moving parts, high-gas–liquid contact area, good mass/heat transfer rates, and large liquid hold-up [1–3]. For processes sensible to shear stress, like those involving cell cultures, BCR's are the most suitable solutions [4,5].

The function of the BCR's may be simply to mix the liquid phase while the gas phase provides agitation, or for mass transfer purposes between phases which is, normally, the most important aim, even though both processes take place simultaneously. The main parameters determining the performance of BCR's are the superficial gas velocity, u_G, the operating pressure and temperature. Besides, there are many variables that also influence bubble column performance such as sparger design (specially in the homogeneous regime) [1], gas hold-up distribution, bubble break-up, coalescence and dispersion rates, bubble rise velocity, bubble size distribution, gas–liquid interfacial area concentration distribution, gas–liquid mass/heat transfer coefficients and the extent of liquid phase backmixing [6,7]. Therefore, in design, scale-up and scale-down, the understanding of the fluid dynamics is a critical issue [8–14]. However, the link between hydrodynamics and mass transfer rates is strong and many times the limiting stage of the processes taking place inside BCR's is mass transfer [15,16]. Thus, the typical design parameter for gas-liquid contact equipment has been the volumetric mass transfer coefficient, k_La [1].

Over the years, apart from empirical correlations based on dimensionless numbers [1,17] the prediction of k_La has been addressed from different theoretical approaches [17]. Among them, the most common nowadays are: (1) the basic model proposed by Kawase et al. [18], combining Higbie's theory [19] with an empirical equation for determining the contact area. (2) An evolution of this method, implementing a population balance model together with Higbie's theory, Shimizu et al. [20] or even coupling them with computational fluid dynamics (CFD) [21]. (3) Another approach is performed by fitting the experimental dissolved oxygen concentrations to mass transfer models. Continuous stirred tank reactor (CSTR) and axial dispersion models (ADM) or its derivatives, slug and cell models, are the most widely used examples of this kind [22–25]. (4) More recently, a model using a Back-Propagation Neural Network based on empirical correlations has been proposed by Lemoine et al. [26] with reasonable results over a wide range of experimental data. However, most of the models rely on adjustable parameters regarding the mass transfer rates.

k_La is function of the contact area between the gas phase and the liquid phase, "a", and the resistance to mass transport in the liquid side, k_L. With reference to the specific contact area, in spite of the fact that bubble shape defines its area, the big number of bubbles with different shapes inside BCR's makes convenient obtaining an average value for the contact area assuming spherical bubbles. However, the effect of bubble shape and deformation on k_L is more critical. As early as 1961, Calderbank and Moo-Young [27] proposed two equations for predicting the Sherwood number for either big

* Corresponding author. Tel.: +34 923294479; fax: +34 923294574.
E-mail address: mariano.m3@usal.es (M. Martín).

1385-8947/$ – see front matter © 2009 Elsevier B.V. All rights reserved.
doi:10.1016/j.cej.2009.01.046

Nomenclature

a	specific contact area (m^{-1})
A	oscillation amplitude
B_i	break-up frequency ($m^{-3}\,s^{-1}$)
clearance	distance between the perforated area and the column diameter (m)
C_{ij}	coalescence frequency for bubbles of class i, j ($m^{-3}\,s^{-1}$)
d_b	bubble diameter (m)
d_e	diameter of the eddies (m)
d_{eq}	equivalent diameter of the bubbles (m)
d_{ij}	diameter of the bubble resulting from coalescence of two (m) defined by Eq. (16)
db_{ini}	bubble diameter at the orifice (m)
D_C	column diameter (m)
$D_L = D_{air-water}$	air diffusivity in water ($m^2\,s^{-1}$)
D_o	orifice diameter (m)
Eo	Eötvös number ($Eo = ((\rho_L - \rho_G)\cdot g \cdot d_{eq}^2)/\sigma$)
Ex	eccentricity; defined by Eq. (52)
f_v	$(d_{b,daughter}/d_{b,mother})^3$
F_n	shape function
g	acceleration due to gravity ($m\,s^{-2}$)
G	generation function defined by Eq. (38)
h_f	final thickness of the drainage film (m)
h_o	initial thickness of the drainage film (m)
I_n	integrals of shape defined by Eqs. (45) and (46)
k	wave number (m^{-1})
k_L	liquid-film resistance ($m\,s^{-1}$)
k_La	volumetric mass transfer coefficient (s^{-1})
$n_{b,i}$	number of bubbles of class i (no. bubbles)
n_e	concentration of eddies per unit volume (no. bubbles m^{-3})
n_i	concentration of class i elements per unit volume (no. bubbles m^{-3})
$n_{orifices}$	actual number of orifices
n_{2Gen}	bubbles of class 2 generated at the sparger (no. bubbles $m^{-3}\,s^{-1}$)
N_e	eddies concentration (eddies kg_{liquid}^{-1})
N_o	number of orifices
N_{oa}	number of orifices per area (m^{-2})
P	hole pitch (m)
P_d	formation period of bubbles (s)
$P_n(x)$	the n degree Legendre polynomial
Pe	Peclet number ($Pe = (u_r \cdot d_b)/D_L$)
Q_c	gas flow rate ($m^3\,s^{-1}$)
r	bubble radius (m)
r_C	column radius (m)
S_{ij}	surface contact area (m^2)
Sh	Sherwood number ($Sh = (k_L d_b)/D_L$)
t	time (s)
t_{ij}	film drainage time (s)
u	generic length units
u_c	critic velocity of a bubble ($m\,s^{-1}$)
u_G	superficial gas velocity ($m\,s^{-1}$)
u_r	rising velocity of a bubble ($m\,s^{-1}$)
u_t	turbulent velocity ($m\,s^{-1}$)
U_l	liquid velocity ($m\,s^{-1}$)
V_b	bubble volume (m^3)
V_s	liquid volume in the column (m^3)
We	Weber number ($We = (d_{eq} \cdot {u_r}^2 \cdot \rho_L)/\sigma$)

Greek symbols

β	parameter for the model by Luo and Svendsen [38]
ε	dissipated turbulent energy ($W\,kg^{-1}$)
ε_g	gas hold-up
θ_{ij}	collision frequency ($m^{-3}\,s^{-1}$)
κ	break-up efficiency
λ_{ij}	coalescence efficiency
λ_n	the tangent to the interphase
μ_G	gas viscosity (Pa s)
μ_L	liquid viscosity (Pa s)
ν_L	kinematic viscosity of the liquid ($m^2\,s^{-1}$)
ρ_G	gas density ($kg\,m^{-3}$)
ρ_L	liquid density ($kg\,m^{-3}$)
σ	surface tension ($N\,m^{-1}$)
τ_{ij}	contact time between bubbles (s)
ω_n	oscillation frequency for the oscillation mode n (Hz)

or small bubbles due to their different behaviour with regard to mass transfer. In spite of the early presentation of the problem, the effect of bubble size and shape has been overlooked as a simplification and few are the theoretical studies for the mass transfer from non-spherical bubbles [28,29]. Thus, most of the equations for implementing the effect of bubble shape and behaviour on k_L rely on adjustable parameters or correlations [18,21,30–35]. The contribution and effect of bubble deformation and shape on the mass transfer rates may be behind the variability of those parameters because bubble oscillations enhance mass transfer rates by modifying the concentration profile surrounding the bubbles [36]. From unveiling that effect, it would be possible to optimise the design of bubble columns.

Therefore, the aim of this paper is to explain the contribution of bubble deformation on the mass transfer from a theoretical point of view in inviscid fluids. The model for the effect of bubble oscillations on the Sherwood number proposed by Montes et al. [36] will be coupled with a population balance based on those used by Pohorecki et al. [11] and Shimizu et al. [20] implementing a new scheme of bubbles to account for the effect of bubble oscillations in mass transfer due to coalescence and break-up processes and to determine the mass transfer rates in bubble column reactors. Experimental results for the volumetric mass transfer coefficient [1,17] and the bubble mean size [17] in bubble columns will be used to establish a comparison and discuss the effect of bubble oscillations on the mass transfer rates. Once the theoretical basis for the effect of bubble oscillations on the mass transfer rates is analyzed in inviscid systems like air–water, the model obtained in this paper will serve as the starting point to understand the effect of the physical properties of the gas–liquid system on the mass transfer rates. Industrial gas–liquid reactors usually operate with complex mixtures where, in many times, water is the solvent (wastewater treatment, fermentations, ...). Coalescence and break-up closures as well as the oscillatory behaviour of the bubbles will be affected by the presence of salts, surfactants or the higher viscosity of the liquid. That will be the aim of further work within the group.

2. Theoretical model

The link between bubble deformation, hydrodynamics and mass transfer is straightforward. On the one hand, inside a bubble column, the fluid flow is responsible for all the processes involving bubbles such as, bubble collisions, break-up, coalescence and detachment. The inertia of each one of these processes induces an initial oscillation amplitude on the bubbles whose characteristics (amplitude and frequency) depend on bubble size and flow regime. On the other hand, the induced bubble deformation modifies the velocity profiles surrounding the bubble

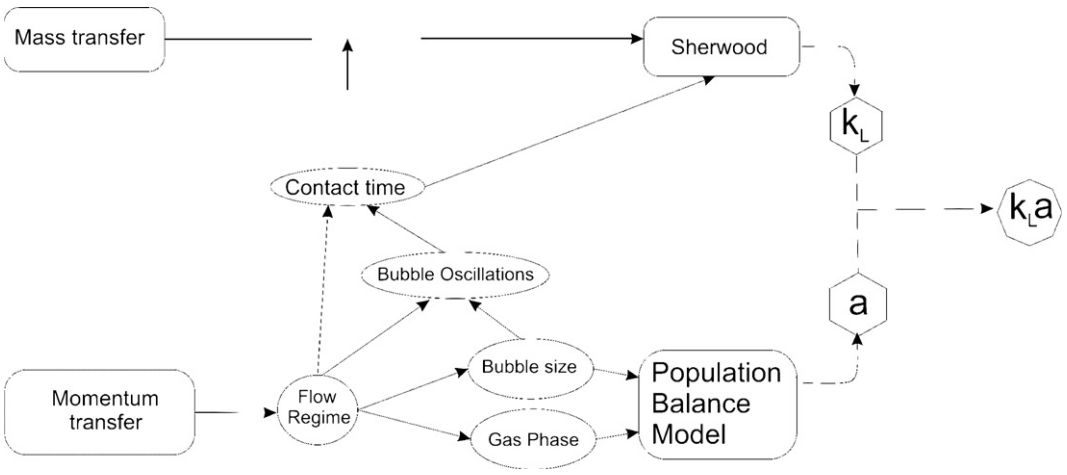

Fig. 1. Scheme for the determination of k_La.

s, the concentration gradients and, thus k_L [36]. Therefore, the loop between hydrodynamics and mass transfer is closed. Fig. 1 shows a scheme of these relationships involving momentum and mass transfer.

Thus, the model consists of two parts. The first is related to modelling the dispersion of bubbles generated in the vessel based on the models proposed by Pohorecki et al. [11] and Shimizu et al. [20]. Bubble formation at the dispersion device, coalescence and break-up processes will be simulated using a population balance which will determine the specific area "*a*" of the dispersion of bubbles. A new scheme of bubbles is proposed to account simultaneously for the effect of bubble break-up and coalescence on the area available and on the oscillation characteristics of the bubbles resulting from those processes. The second part is the determination of the liquid-film resistance, k_L. The physical properties of the gas–liquid system and bubble size will allow determining their oscillation amplitude which defines the Sherwood number of each bubble size [36]. By combining k_L and a, k_La is calculated.

2.1. Hydrodynamics

Fluid hydrodynamics involves the processes related to bubble formation, rising, coalescence and break-up. Bubble formation at the orifice will be the starting point to determine the dispersion of bubbles. Different closures for bubble coalescence and break-up will be checked [13,37–40] to obtain a bubble size distribution that matches the experimental one, verifying the bubble scheme.

2.1.1. Bubble scheme

In most of the studies on bubble dispersions, a number of bubble classes/sizes is defined in advance. The bubbles resulting from coalescence and break-up processes are reorganized to fit the predefined classes. This fact not only leads to problems regarding the total gas phase in the tank, but, above all, results in difficulties when determining the effect of bubble coalescence and break-up on the mass transfer. For instance, coalescence decreases the gas–liquid contact area meanwhile the bubble resulting from coalescence presents a bigger oscillation amplitude. From the balance between these two hydrodynamic effects, the mass transfer rates may be reduced depending on the size of the bubbles involved [41]. To account for this effect, we propose a scheme of bubbles, shown in Fig. 2, so that the bubbles resulting from coalescence and break-up processes exist.

For the sake of simplicity in plotting the scheme of the bubbles present in the bubble column, Fig. 2, we consider that the initial bubble size at the sparger, which actually depends on the orifice size and the gas flow across, has a volume of 16 u^3.

(a) A range of orifices (d_o) from 0.001 to 0.01 m will be tested even though 0.005 m orifices are preferred in industry [42]. Small

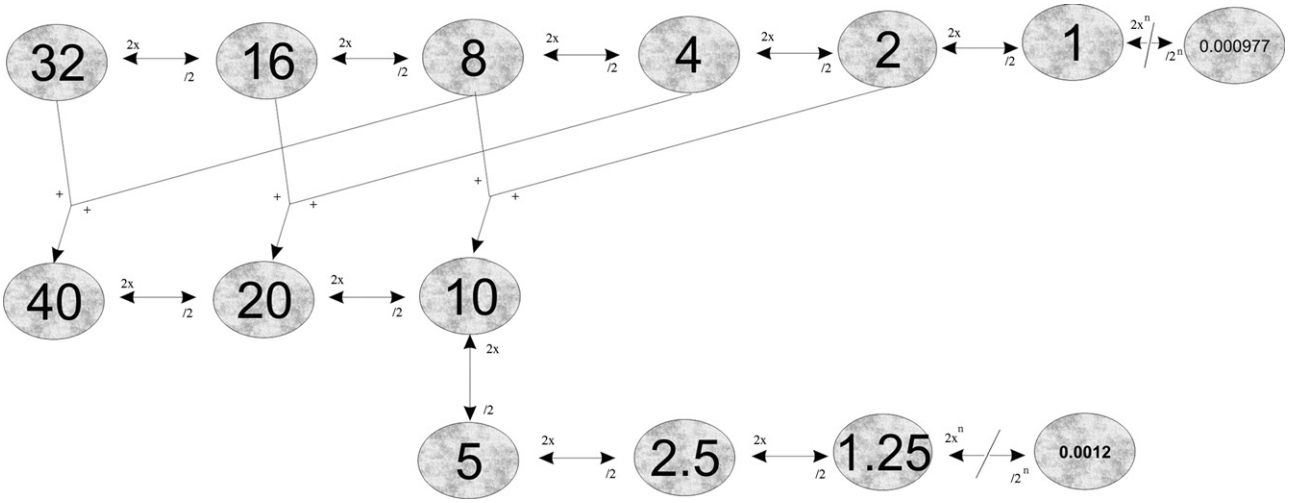

Fig. 2. Scheme of normalized bubbles in the dispersion generated in a bubble column.

orifices of 0.001 or 0.002 m, like the ones typically used in laboratory scale columns, present corrosion problems. Meanwhile, larger holes are occasionally used for fouling systems.

(b) Bubble size at the orifice will be calculated using a correlation developed from experimental results obtained in previous papers by the authors, regarding the effect of orifice size in bubble volume [43] as well as the effect of the gas flow rate [44]. With those results we can propose Eq. (1) for bubble size at the orifice:

$$db_{ini} = (138 \cdot d_o) \cdot \left(\frac{Q_c}{N_o}\right)^{0.26} \quad (1)$$

(c) The number of orifices in the dispersion device, N_o, depends on the configuration of the sieve plate. Holes are usually placed on 60° equilateral triangular pitch with the liquid flowing normally [45]. Holes spaced closer than twice the hole diameter lead to unstable operation. Therefore, the recommended spacing is $2.5d_o$ to $5d_o$. In this paper $3.5d_o$ will be used [2,46]. According to this typical configuration the number of orifices in a sieve plate is given by Ludwig [45]:

$$N_{oa} = 1.158 \cdot \left(\frac{P}{0.0254}\right)^{-2}; \quad (2)$$

$$N_o = N_{oa} \cdot \left(\pi \cdot \left(\frac{D_c - clearance}{2}\right)^2\right); \quad (3)$$

Clearance will be 5% of D_c (D_c = 1 m).

Following these rules for designing sieve plates, it is important to point out that the gas flow rate per orifice in a bubble column operating in the homogeneous regime is within the range of gas flow rates used in the experiments [43,44]. Therefore, Eq. (1) can be used.

From the initial bubble size at the orifice (normalized volume of 16 u^3), bubble coalescence and break-up processes are allowed subjected to certain conditions to obtain different bubble classes/sizes. The actual bubble sizes in the column are represented in Fig. 2. The processes allowed (coalescence and break-up) are represented as arrows linking the bubbles sizes, circles, under consideration for each single process, with the operators used attached to the tip of the arrow defining the process ((2×) to identify that two bubbles of the smaller bubble will give another of the bigger volume, (/2) to talk about binary break-up of the bubbles into two equal ones or an operator (+) is located to say that those two bubbles will coalesce).

In particular, regarding coalescence, two bubbles of the same size will be allowed to coalesce to obtain a bubble of twice its initial size. For example, a bubble of volume 8 u^3 can merge with another one of the same size (2×) to obtain a bubble of volume 16 u^3. The arrow points from the circle with 8 to the circle with 16 with the operator (2×) plotted on the tip to define this coalescence process. For bubbles of different sizes, the coalescence processes are limited to those in which the circles are linked and an operator (+) is added to the arrows. For instance, a bubble of size 4 u^3 can merge with another of size 16 u^3 to obtain another of 20 u^3.

In order to determine the probability of coalescence, different mechanisms are considered. For bubbles of the same size, only laminar and turbulent collisions are used since they are supposed to have the same rising velocity. No wake effect is considered. For coalescence between bubbles of different sizes, buoyancy collision is also considered.

Only binary break-up into two daughter bubbles is considered for all bubble sizes, since it is overwhelmingly the major break-up manner supported by experimental observations [47–49] Furthermore, it will be assumed that a bubble breaks into two equal size daughter bubbles, which has proved to be successful in modelling the hydrodynamics of bubble columns [11,20] and stirred tanks [50]. Eq. (4) allows determining the volume of the bubbles generated in the break-up. For example, a bubble of normalized volume of 8 u^3 can be broken into two equal ones of 4 u^3. This process is represented in Fig. 2 by an arrow pointing from the circle with number 8 to the circle with number 4 and an operator (/2) indicating that the bubble splits into two. Thus, the volume of the bubbles is calculated as follows:

$$2 \cdot \frac{4}{3}\pi\left(\frac{d_{b,j+1}}{2}\right)^3 = 2 \cdot V_{b,j+1} = V_{b,j} = \frac{4}{3}\pi\left(\frac{d_{b,j}}{2}\right)^3 \quad (4)$$

These simplifications will allow handling the effect of bubble break-up in generation of area and on the effect of bubble oscillations on the mass transfer, while maintaining the total gas phase monitored.

In order to simulate bubble break-up and coalescence, we are going to introduce the closures used in this model. Due to the particular scheme of bubbles proposed, different closures are going to be tested to simulate the bubble size distribution.

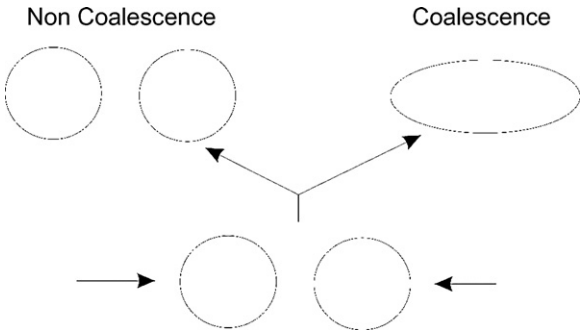

Fig. 3. Collision process of bubbles.

2.1.2. Bubble coalescence

Inside a column, the flow field leads to bubble collision. After the collision of two bubbles, a drainage channel is developed and the liquid-film between the bubbles is partially or totally drained, in which case bubbles coalesce. Fig. 3 shows both possibilities. For mass transfer processes, it is important to highlight that in case of bubble coalescence, there is a decrease in gas–liquid contact area. At the same time, the inertia of the process makes the resulting new bubble oscillate, looking for an equilibrium shape in accordance with the new size, enhancing mass transfer rates [36]. From the balance between these two effects, the mass transfer rate may decrease or not, depending on the size of the bubbles involved [41]. Thus, it is important to implement both effects when modelling mass transfer in bubble columns. Meanwhile, in absence of coalescence, bubble collisions provide with initial oscillation amplitude.

The model for bubble coalescence is based on the study of the collisions of the bubbles. Different mechanisms are responsible for bubble collision. However, not every collision leads to coalescence. Therefore, Prince and Blanch [37] proposed a model for bubble coalescence in bubble columns where the coalescence rate, C_{ij} (m^{-3} s^{-1}), for two bubbles i, j whether they are of the same class (i=j) or not ($i \neq j$), is given by the product between the collision frequency and the efficiency by which that collisions derive in coalescence Eq. (5).

The total collision frequency is reported to be the sum of different mechanisms, such as turbulent, buoyancy and laminar stress collisions, see Eq. (5). Each mechanism is labelled with a superindex, indicating the physical process from which it is derived [37]:

$$C_{ij} = (\theta_{ij}^T + \theta_{ij}^B + \theta_{ij}^{LS}) \cdot \lambda_{ij} \quad (5)$$

Among the collision mechanisms, θ_{ij}^{T} corresponds to the collision frequency between two bubbles in turbulent regime due to the relative motion of the bubbles. It is based on the collision theory for ideal gases where concentration, bubble size and velocity can be arranged as the expression given by Eq. (6) [37]:

$$\theta_{ij}^{T} = n_i \cdot n_j \cdot S_{ij} \cdot (u_{ti}^2 + u_{tj}^2)^{0.5} \tag{6}$$

The collision cross sectional area, S_{ij}, between bubbles is defined as Eq. (7) [20]:

$$S_{ij} = \frac{\pi}{16}(d_{bi} + d_{bj})^2 \tag{7}$$

The turbulent velocity, u_t, for bubbles of diameter d_b in the inertial subrange of isotropic turbulence is [51]

$$u_t = 1.4 \cdot \varepsilon^{1/3} \cdot d_b^{1/3} \tag{8}$$

where ε is the dissipation energy. Meanwhile, n_i represents the number of bubbles of class i per unit volume.

Another typical collision mechanism is that which occur when a bubble reaches another bubble [37]:

$$\theta_{ij}^{B} = n_i \cdot n_j \cdot S_{ij} \cdot (u_{ri} - u_{rj}) \tag{9}$$

The rising velocity, u_{ri}, can be calculated following Eq. (10) [37]:

$$u_{ri} = \left(2.14 \cdot \frac{\sigma}{\rho_L \cdot d_{bi}} + 0.505 \cdot g \cdot d_{bi}\right)^{0.5} \tag{10}$$

Laminar stress collision rate, θ_{ij}^{LS}, occurs when a bubble overtakes another bubble. The collision rate due to laminar shear can be expressed as Eq. (11) [52]:

$$\theta_{ij}^{LS} = n_i n_j \cdot \frac{4}{3} \cdot \left(\frac{d_{bi}}{2} + \frac{d_{bj}}{2}\right)^3 \cdot \left(\frac{\mathrm{d}U_l}{\mathrm{d}r_C}\right) \tag{11}$$

where the shear rate can be expressed as follows [37]:

$$\left(\frac{\mathrm{d}U_l}{\mathrm{d}r_C}\right) \approx \frac{U_l}{D_C/2} = \frac{0.787(g \cdot D_C u_G)^{1/3}}{D_C/2} \tag{12}$$

where D_C is the diameter of the BCR. We are going to consider D_c to be equal to 1 m.

However, not every collision results in coalescence. Coalescence probability depends on the intrinsic contact between bubbles. Coulaloglou and Tavlarides [53] defined the collision efficiency between bubbles of classes i and j, λ_{ij}, as a probability function given by Eq. (13) which depends on the relationship between the time required for film drainage, t_{ij}, and the contact time of the bubbles, τ_{ij}:

$$\lambda_{ij} = \exp\left(-\frac{t_{ij}}{\tau_{ij}}\right) \tag{13}$$

Contact time can be calculated through Eq. (14) [37]:

$$\tau_{ij} = \frac{(0.5 \cdot d_b)^{2/3}}{\varepsilon^{1/3}} \tag{14}$$

In our work, the drainage time can be calculated as Eq. (15) [37], which is a modification of that developed by Marrucci et al. [54]:

$$t_{ij} = \left(\frac{(0.5 \cdot d_{ij})^3 \cdot \rho_L}{16 \cdot \sigma}\right)^{0,5} \cdot \ln\left(\frac{h_0}{h_f}\right) \tag{15}$$

where

$$d_{ij} = \left(\frac{2}{d_{bi}} + \frac{2}{d_{bj}}\right)^{-1} \tag{16}$$

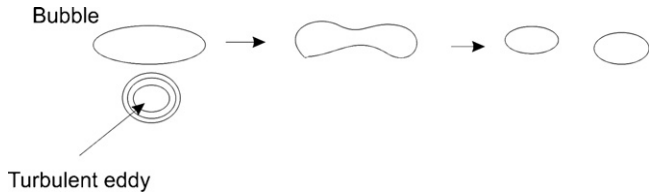

Fig. 4. Bubble deformation and break-up in turbulent flow.

In accordance with the results gathered by Prince and Blanch [37]:

$$\begin{aligned} h_0 &= 1 \times 10^{-4}\ \mathrm{m} \\ h_f &= 1 \times 10^{-8}\ \mathrm{m} \end{aligned} \tag{17}$$

Due to the particular scheme of bubbles, different closures will be used to model the bubble size distribution. Lou and Svendsen [38] proposed an alternative model for the turbulent collision rate that can be written as Eq. (18) for a discrete system of bubbles:

$$\theta_{i,j}^{T} = \frac{\pi}{4}\sqrt{2}\varepsilon^{1/3}(d_{b,i}+d_{b,j})^2(d_{b,i}^{2/3}+d_{b,j}^{2/3})^{1/2} \cdot e^{[(-We_{i,j}^{1/2}(0.75\cdot(1+(d_{bi}/d_{bj})^2)\cdot(1+(d_{bi}/d_{bj})^3))^{0.5})/((1+(d_{bi}/d_{bj})^3)(\rho_G/\rho_L+0.5))]} \tag{18}$$

The Weber number of the bubbles can be calculated using Eq. (19):

$$We_{i,j} = \frac{\rho_L \cdot d_{b,i} \cdot u_{t,(i,j)}^2}{\sigma} \tag{19}$$

Meanwhile, the turbulent velocity is calculated using the turbulent velocity of each colliding bubble

$$u_{t,(i,j)} = (u_{t,i}^2 + u_{t,j}^2)^{0.5} \tag{20}$$

2.1.3. Bubble break-up

The energy dissipated in the flow deforms and eventually breaks the bubbles, see Fig. 4. The bubbles resulting from that breakage oscillate as a result of the inertia of the process. Therefore, break-up not only generates contact area but also enhances the mass transfer rates by deforming the bubbles.

Different bubble breakage rates from the literature are used to obtain a modelled bubble size distribution that matches the experimental one following the scheme of bubbles presented in Fig. 2.

(a) Prince and Blanch [37] modelled bubble breakage due to bubbles colliding with turbulent eddies. Therefore, the break-up rate is written as the product between the collision rate of bubbles and turbulent eddies and the efficiency of those collisions. Thus, the break-up frequency is

$$B_i = \theta_{ie} \cdot \kappa_i \tag{21}$$

The collision velocity of turbulent eddies and bubbles is based on the same mechanism explained for bubble collision assuming that the eddies behave as entities [37]:

$$\theta_{ie} = n_i \cdot n_e \cdot S_{ie} \cdot (u_{ti}^2 + u_{te}^2)^{0.5} \tag{22}$$

The turbulent velocity of the eddies can be written as Eq. (24) [37]:

$$u_{te} = 1.4 \cdot \varepsilon^{1/3} \cdot d_e^{1/3} \tag{23}$$

Using Kolmogorov's theory of isotropic turbulence, the size of the eddies, d_e, generated in the tank can be calculated by Eq.

(24) [11]:

$$d_e = \left(\frac{\nu_L^3}{\varepsilon}\right)^{0.25} \tag{24}$$

and the cross-sectional area [11]:

$$S_{ie} = \frac{\pi}{16}(d_{bi} + d_e)^2 \tag{25}$$

An expression for the number of eddies as function of the wave number is given by Eq. (26) [11]:

$$\frac{dN_e(k)}{dk} = 0.1 \cdot \frac{k^2}{\rho_L} \tag{26}$$

where the wave number is [11]

$$k = \frac{2}{d_e} \tag{27}$$

The differential equation has to be solved using as lower and upper limits those given by Pohorecki et al. [11]. Only the eddies from $0.2d_b$ to d_b can actually break the bubbles. Smaller eddies do not have enough energy; meanwhile bigger ones drag the bubbles across the vessel [37]. Therefore, as a mean value, $d_e = 0.6d_b$ as has been proved valid for modelling bubble break-up [50]:

$$N_e = 0, \quad k = \frac{2}{0.2 \cdot d_b} \tag{28}$$

$$N_e = N_e, \quad k = \frac{2}{d_b} \tag{29}$$

Vortex concentration per unit volume of liquid is

$$n_e = N_e \cdot \rho_L \tag{30}$$

Bubble break-up in bubble columns occurs when the liquid turbulence is high enough to deform the bubbles heavily above their stable point, which depends on the physical properties of the liquid and on the fluid flow. Therefore, it is necessary to determine which eddies have enough energy to break the bubbles. Bubble break-up efficiency can be written as Eq. (31) [11]:

$$\kappa_i = \exp\left(-\frac{u_{ci}^2}{u_{te}^2}\right) \tag{31}$$

where the critical vortex velocity capable of breaking a bubble of diameter d_{bi} [11,37] is given as follows:

$$u_{ci} = \left(\frac{We_c \cdot \sigma}{d_{bi} \cdot \rho_L}\right)^{0.5} \tag{32}$$

The Weber critical number (We_c) can be found to be from 0.5 to 7.8 according to different authors [55,56]. The value originally used by Prince and Blanch [37] was 2.3. However, Shimizu et al. [20] used $We_c = 1$ in his model. Therefore, We_c will be the parameter of the model to account for bubble stability under the experimental conditions.

Due to the particular scheme of bubbles, different closures from the literature will also be checked to simulate bubble size distribution verifying the scheme of bubbles proposed to account for the effect of bubble break-up and coalescence on bubbles oscillation and mass transfer rates shown in Fig. 2.

(b) Luo and Svendsen [38] proposed another model for the break-up frequency which accounts for the total gas phase in the BCR. It depends on a parameter $\beta = 2.045$. In order to implement the model of Luo and Svendsen [38], the authors also solve the distribution of bubbles obtained after bubble break-up. However, as it was explained in Section 2.1(a), we are going to assume the scheme of bubbles show in Fig. 2 where bubbles break in two equal bubbles. Besides $d_e = 0.6d_b$. With these assumptions, the original break-up frequency becomes

$$B_i = 0.923(1-\varepsilon_g)\left(\frac{\varepsilon}{d_b}\right)^{1/3}\frac{(1+(d_e/d_b))^2}{d_b^2(d_e/d_b)^{11/3}} \cdot e^{[(-\pi\sigma d_b^2(j)(f_v{}^{2/3}+(1-f_v)^{2/3}-1))/(\pi\rho_L\beta/12(d_e/d_b)^{11/3}(d_b\varepsilon)^{2/3})]} \tag{33}$$

(c) Martínez-Bazán et al. [57,58] developed another model for bubble break-up efficiency based on the stability of a jet. The forces under consideration are those which maintain bubble size, surface tension, and those which attempt to deform it, the turbulent energy. The model proposed considers that the bubbles have the bigger probability of break into two equal daughter bubbles. The constant 8.2 was determined by Batchelor [59] meanwhile 0.25 a characteristic value for the air–water system experimentally obtained by the authors [57,58]:

$$B_i = n_i \cdot 0.25\frac{\sqrt{8.2(\varepsilon \cdot d_{b,i})^{2/3} - 12\sigma/(\rho_L d_{b,i})}}{d_{b,i}} \tag{34}$$

2.1.4. Energy dissipation

Energy in the tank is responsible for bubble collisions and deformation as well as for maintaining bubble oscillation. It is traditionally considered that the dissipated energy can be defined by Eq. (35) used by Shimizu et al. [20] and Pohorecki et al. [11]:

$$\varepsilon = u_G \cdot g \tag{35}$$

2.1.5. Dispersion generated

A population balance based on that proposed by Fleischer et al. [60] will determine the fraction of bubbles of each size:

$$\frac{\partial}{\partial t}n(z,d_b,t) + \frac{\partial}{\partial z}[n(z,d_b,t)u_r(z,d_b)] + \frac{\partial}{\partial d_b}\left[n(z,d_b,t)\frac{\partial}{\partial t}d_b(z,d_b)\right] = G(z,d_b,t) \tag{36}$$

In a stationary regime Eq. (36) becomes [11]

$$0 = G(z,d_b,t) \tag{37}$$

G represents a balance between the coalescence and break-up processes [11]. In our case the function G is as follows:

$$G_i = \frac{1}{2}\sum_{k=1}^{2}\sum_{l=1}^{2}C_{i,kl} - \sum_{j=1}^{2}C_{ij} + 2 \cdot B_{i-1} - B_i \tag{38}$$

Bubbles are periodically generated at the dispersion device (primary bubbles or bubbles of class 1), so that Eq. (38) must be completed by Eq. (41) when applied for this bubble class, to account for their presence in the tank due to the bubbling process:

$$n_{2Gen} = \frac{n_{orifices}}{V_s \cdot P_d} \tag{39}$$

where V_s corresponds to the liquid volume of study and P_d is the formation period of the bubbles in each experimental condition.

Eq. (37) will be applied for 30 real bubble classes. So, the model consists of 30 equations like that given by Eq. (37) where the break-up and coalescence rates have been defined by the equations presented along the paper.

In order to solve the hydrodynamic model, the total number of bubbles in the column will be determined by the gas hold-up. According to the theoretical model proposed so far, a theoretical expression for the gas hold-up is required. The model proposed by Kawase and Moo-Young [61], based on the concept of a characteristic turbulent kinematic viscosity, can be used. However, in order to

reduce the error when comparing experimental and calculated k_La, it is interesting to use a correlation for ε_g determined for the same experimental device and conditions as those used when determining k_La. Therefore, the correlation proposed by Akita and Yoshida [62] has been used. Akita and Yoshida [62] also provide values for the specific contact area "a", bubble mean diameter, and k_La, which are necessary for the validation of the model. In this way, no error related to the bubble dispersion generated can be considered since the model will simulate the hydrodynamics for which the k_La had been measured. Eq. (40) has been used for ε_g:

$$\frac{\varepsilon_g}{(1-\varepsilon_g)^4} = 0.2 \cdot \left(\frac{9.8 \cdot D_c \cdot \rho_L}{\sigma}\right)^{1/8} \cdot \left(\frac{g \cdot D_c^2 \cdot \rho_L^2}{\mu_L^2}\right)^{1/12} \left(\frac{u_G}{\sqrt{D_c \cdot g}}\right) \tag{40}$$

The number of bubbles of each class is calculated as a fraction of the total gas phase:

$$n_{b,j} = \frac{3 \cdot \varepsilon_g \cdot D_c^2 \cdot (4 \cdot D_c + Vol_{gas}/(\pi(D_c/2)^2))}{2 \cdot d_{b,j}^3} \cdot x_j \tag{41}$$

The bubble fraction of class i, x_j, must be calculated. In order to do so, only the homogeneous regime is going to be considered. It has been proved that the experimental monomodal distributions of bubbles in stirred tanks and bubble columns can be adjusted to a log-normal distribution [11,37,50]. Therefore, a log-normal distribution for the bubbles in the column is considered whose parameters μ_{dist} and σ_{dist} will be found from minimizing Eq. (47):

$$\sum G_i = 0 \tag{42}$$

It should be highlighted that the purpose of this work is not to study the effect of the different closures when modelling the hydrodynamics since better works have been developed for such purpose, i.e. [13], but to determine the mass transfer once the experimental bubble size distribution is simulated. However, the proposed scheme of bubbles suggests that different closures are checked to model the bubble size distribution.

2.1.6. Experimental results

The mean diameter of a dispersion calculated using the model will be compared with the experimental correlation given by Eq. (43) [62]:

$$d_{32} = 26 \cdot D_c \cdot \rho_L \cdot \left(\frac{g \cdot D_c^2 \cdot \rho_L}{\sigma}\right)^{-0.5} \cdot \left(\frac{g \cdot D_c^3}{(\mu_L/\sigma)^2}\right)^{-0.12} \cdot \left(\frac{u_G^2}{g \cdot D_c}\right)^{-0.06} \tag{43}$$

2.2. Mass transfer

2.2.1. Sherwood number of oscillating bubbles

Bubble behaviour in process vessels depends on its size [27]. Big bubbles are deformable and can oscillate in the flow so that, apart from providing contact area, they have another contribution to the mass transfer rate, the modification of the concentration profiles surrounding the bubbles as a result of bubble oscillations. Bubble oscillations depend on the physical properties of the gas–liquid system, bubble size and the energy available in the system. To account for this contribution, Montes et al. [36] developed a model for the Sherwood number as function of bubble oscillations:

$$Sh = \frac{2}{\sqrt{\pi}} Pe^{1/2} \left[I_{n1} + I_{n2} \frac{A}{\omega_n^2} We^{1/2}\right] \tag{44}$$

where I_{n1} and I_{n2} are constants that depend on the geometry of the bubble:

$$I_{n1} = \frac{3}{4\pi\sqrt{2}} \int_0^{\pi} \int_0^{\pi} N(\theta) \frac{\partial r}{\partial \nu} \left[F_n^2 + \left(\frac{\partial F_n}{\partial \theta}\right)^2\right]^{1/2} \sin\theta \, d\theta \, dt \tag{45}$$

$$I_{n2} = \frac{3}{8\pi} \int_0^{\pi} \int_0^{\pi} N(\theta) \frac{\partial r}{\partial \nu} \left[F_n^2 + \left(\frac{\partial F_n}{\partial \theta}\right)^2\right]^{1/2} \sin\theta \, d\theta \, dt \tag{46}$$

These equations are valid for every oscillation mode, where the radial derivative in the normal direction to the bubble surface is given by

$$\frac{\partial r}{\partial \nu}(\theta, t) = \frac{1}{||\cos[\theta + \tan^{-1}(\lambda_n)]||} \tag{47}$$

which is the derivative in the radial direction with respect to the normal surface of the bubble for each bubble point. And λ_n is the tangent to the interphase at each point of the bubble surface:

$$\lambda_n = \frac{F_n + \cos\theta(dF_n/d\cos\theta)}{\sin\theta(dF_n/d\cos\theta) - (F_n/\tan\theta)} \tag{48}$$

with:

$$F_n(\theta, t) = 1 + AF_n^1(\theta, t) + \cdots, \tag{49}$$

$$F_n^1 = \cos(t) \cdot P_n(\cos\theta) \tag{50}$$

$P_n(\cos\theta)$ is the n degree Legendre polynomial. The amplitude of the oscillation, A, is defined by Eq. (51) [63]:

$$A = \frac{d_{max} - d_{min}}{2d_{eq}} \tag{51}$$

To determine bubble oscillation amplitude of each bubble size in the dispersion, the maximum and minimum diameters of a bubble are needed. Both are related to bubble deformation. Considering that a bubble during an oscillation is an ellipsoid, both diameters can be related to the eccentricity defined by means of Eötvös number [34]:

$$Ex = \frac{1}{1 + 0.163 \cdot Eo^{0.707}} \tag{52}$$

Therefore, the oscillation amplitude can be written as

$$A = \frac{1 - Ex}{2 \cdot Ex^{1/3}} \tag{53}$$

According to Eq. (53) bubble oscillation amplitude increases with bubble diameter, in accordance with the experimental results from Montes et al. [36].

$N(\theta)$ is a dimensionless geometrical function depending on the angular coordinate, θ, of each point in the bubble surface, defined by Eq. (54) [36]:

$$N(\theta) = \frac{\sin^2\theta}{(1 - (3/2)\cos\theta + (1/2)\cos^3\theta)^{1/2}} \tag{54}$$

Koynov et al. [64] found that in bubble swarms, bubbles no longer traveled by themselves, but rather in liquid perturbed by the wakes of neighboring bubbles. In addition, the concentration of gas dissolved in the liquid around the bubble in a swarm no longer depended only on the mass transfer from the bubble itself, but also on the mass transfer from the other bubbles in the swarm. These two factors resulted in a decrease in the mass transfer coefficient of the bubble swarm compared with a single bubble. Therefore, it is considered that k_L theoretically obtained for one single bubble

cannot be used in a dispersion of bubbles because the presence of other bubbles does not allow the complete development of the velocity and concentration gradients surrounding a bubble. A correction factor is applied. The theoretical one reported by Lamont and Scott [30], 0.4 has been used.

2.2.2. Volumetric mass transfer coefficient

The volumetric mass transfer coefficient, k_La, is calculated as the product between the liquid-film resistance obtained from the Sherwood number of each bubble class and the contact area provided by the number of bubbles of that class extended to all bubble class in the dispersion generated in the column. Eq. (55) shows this calculus:

$$k_La = \sum_{i=1}^{30} \frac{Sh \cdot D_{airwater}}{d_{b,i}} \cdot \sum n_i \cdot 4\pi \cdot \left(\frac{d_{b,i}}{2}\right)^2 \quad (55)$$

2.2.3. Experimental data for k_La

Experimental results from the literature have been used to validate the model. The first correlation was obtained for sieve plates is [1]

$$k_La = 0.467 \cdot u_G^{0.82} \quad (56)$$

The equation obtained by Akita and Yoshida [17] has also been used.

$$k_La = 0.6 \cdot \frac{D_L}{D_c} \cdot \left(\frac{\mu_L}{D_L \cdot \rho_L}\right)^{0.5} \left(\frac{g \cdot \rho_L}{\sigma}\right)^{0.62} \left(\frac{g}{(\mu_L/\rho_L)^2}\right)^{0.31} \varepsilon_g^{1.1} \quad (57)$$

where ε_g is given by Eq. (40).

3. Comparison between experimental and simulated results

The model simulates, first, the dispersion of bubbles generated in the column and second, k_La, by combining the contact area given by the dispersion of bubbles and the liquid-film resistance of each bubble size in the vessel.

Before attempting to simulate the experimental results, the reported effect of the orifice size of the sparger on k_La [1] has been analyzed. Orifices ranging from 0.001 to 0.01 m are considered for different superficial gas velocities in the homogeneous regime.

It is reported that the dispersion device also determines k_La [1]. Therefore, the effect of different orifice sizes is going to be simulated to study its effect on the mean size of the bubbles in the dispersion.

Fig. 5 shows the sauter mean diameter, d_{32}, calculated using different break-up and coalescence closures, versus the orifice diameter for a small gas flow rate, $u_G = 0.001\ m\ s^{-1}$. It can be seen that for small initial bubble diameter, like the ones generate from orifices smaller than 0.003 m, the resulting mean bubble size in the dispersion depends on the sparger. Bubbles are stable in the flow due to their size and the low energy available. However, for a certain orifice size, the initial bubble size is unstable and the energy dissipated in the tank will determine bubble mean size of the dispersion. Even though, a value of u_G as low as $0.001\ m\ s^{-1}$ is too small to be used in a column, and the results are shown only to highlight that the contribution of the dispersion device is only important if it generates small stable bubbles.

For a common superficial gas velocity in the homogeneous regime, $u_G = 0.01\ m\ s^{-1}$, Fig. 6 plots d_{32} versus the initial orifice diameter for different break-up and coalescence closures. In Fig. 6 it can be seen that bubble mean size is mainly determined by the energy dissipated in the flow for the typical bubble sizes at the orifice. The variability with respect to a constant value can be related more to the numerical solution than to physical meaning.

The dependence of the bubble mean size on either the dispersion device or on the energy dissipated in the tank, explains the differences in the correlations for k_La found for different dispersion devices, porous plates and sieve plates [1]. In summary, if the generated bubbles at the sparger are really small, it is the sparger which defines bubble dispersion in the tank. Otherwise, the dissipated energy is responsible for the bubble mean size. This fact translates into an effect on k_La. That is the theoretical explanation for the results of previous experimental studies [1,41] where smaller bubble mean diameter resulted in bigger proportional constants in equations like Eq. (56).

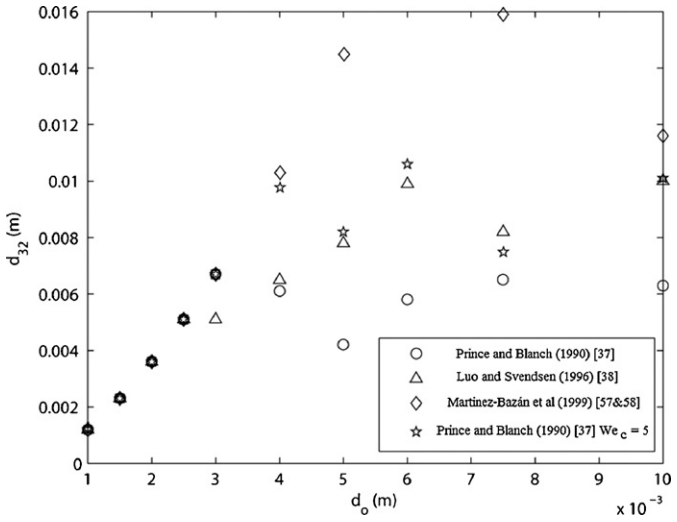

Fig. 5. Effect of the dispersion device in bubble mean size of a dispersion.

Thus, assuming that the only important contribution to the mean diameter of the dispersion is the energy dissipated in the column, under the experimental conditions investigated, a mean d_{32} value is obtained for $d_o = 0.005$ m, the preferred hole size in industry. Fig. 7 plots the mean diameter obtained using different break-up and coalescence closures versus u_G. Experimental results from the literature have also been used. In general, the different closures show an important disagreement among each other, as other authors have pointed out [13,40]. In general, one of the reasons behind that disagreement is the scheme of bubbles proposed to account for the effect of bubble deformation on the mass transfer rates.

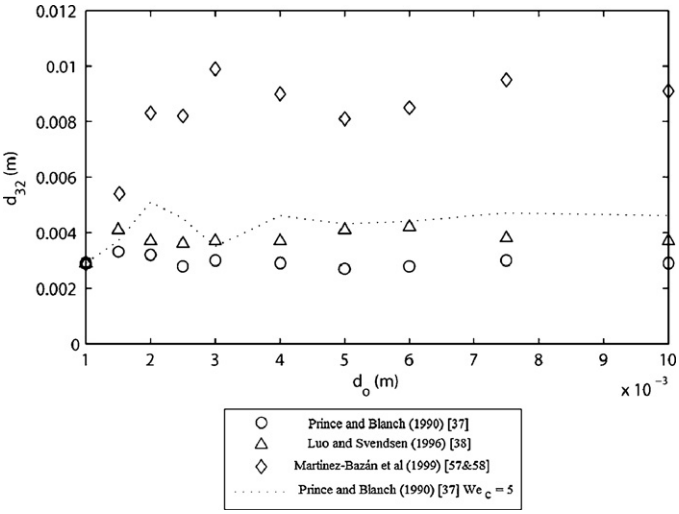

Fig. 6. Effect of break-up and coalescence closures on bubble mean diameter of the dispersion $u_G = 0.01\ m\ s^{-1}$.

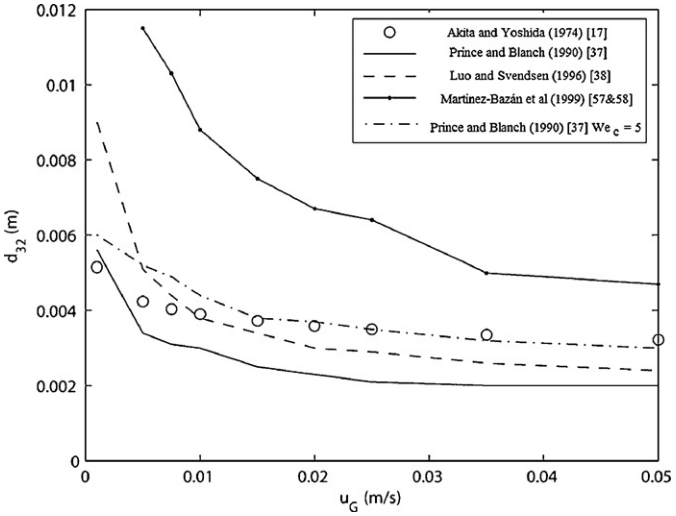

Fig. 7. Optimization of the We_c.

In particular, it is worth mentioning that the bubble size distributions predicted by the model of Prince and Blanch [37] have a mean value smaller than the experimental results and approach the equilibrium distribution fast. This is caused by the high-bubble break-up rate. On the contrary, the break-up rate predicted by Lasheras et al.'s [39] model reveals low-bubble break-up rates leading to bigger mean size bubbles. When using the coalescence and break-up rates proposed by Luo and Svendsen [38], the model results in values closer to the experimental ones but smaller too. The lack of agreement when using the model by Luo and Svendsen [38] was to be expected because they consider that a bubble is more likely to break in a big and a small daughter bubbles rather than two equal ones as has been assumed in this work.

According to Hinze's work [55], the Weber critical number is a measure of the stability of the particles, either drops or bubbles, and depends on the physical system and the break-up mechanisms [50,55]. Therefore, based on Prince's model for the break-up rate, We_c has been used as a parameter which will help understand bubble dispersions. $We_c = 5$ turn out to be the best result to simulate the bubble mean diameter using the bubble scheme proposed, compared to the experimental results provided by Eq. (43). Fig. 7 shows the results.

In order to explain and predict mass transfer rates, it is only reasonable to use the hydrodynamics that matches the experimental results considering the bubble scheme proposed in this paper. From now on, only the model using Prince and Blanch's [37] equations and $We_c = 5$, will be further used to study the mass transfer rates form oscillating bubbles.

k_La depends on bubble size in order to define the contact area "a" and "k_L". According to Fig. 6, we can consider that the bubble size does not depend on the dispersion device as long as the initial bubble size is big enough to be broken in the flow. Therefore, for each u_G, the bubble dispersion is simulated solving Eq. (41). k_L is calculated using the model proposed by Montes et al. [36] for each bubble size where the characteristic amplitude is determined using Eqs. (52) and (53). Fig. 8 shows the comparison between the experimental results using Eqs. (56) and (57) and the theoretically predicted by the model.

The different values for correcting k_L [18,21,30–35] can be explained based on the effect of bubble deformation on the mass transfer rates due to the oscillation of the bubbles. It is important to point out that the better the fitting between the experimental and the modelled mean diameter, the better the fitting between the calculated and experimental k_La (values for $u_G = 0.015$–$0.025\ \mathrm{m\,s^{-1}}$).

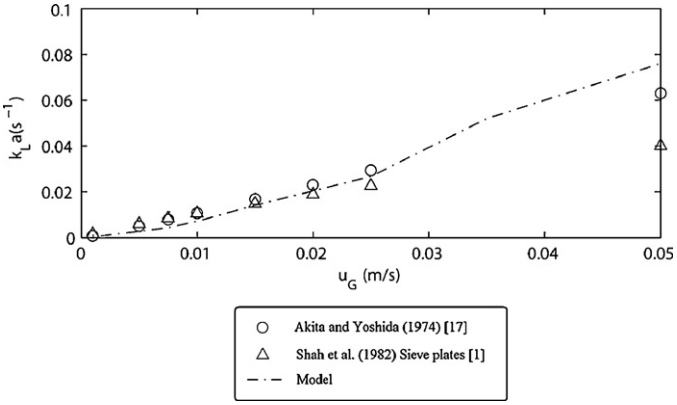

Fig. 8. Comparison between the experimental and the modelled values for k_La.

4. Conclusions

Bubble column design is a key issue for the chemical and biochemical industries due to the wide range of application. So far, different adjustable parameters have been used to fit the experimental values of bubble diameters and k_La and the theoretical ones. The physical meaning of the theoretical parameters of the model allows a better understanding of the operation of bubble columns.

The effect of the dispersion device is only of importance either in case of low-dissipated energies or when really small bubbles are generated at the dispersion device. In both cases the bubbles are stable in the flow.

Predicting bubble mean size in a vessel is sensitive to the break-up and coalescence closures and has an important impact on the volumetric mass transfer coefficient due to the fact that bubble size determines not only the contact area between the phases but also the liquid-film resistance. The hydrodynamics in the column was modelled based on the fact that bubble stability in the flow is what determines bubble break-up. We_c has been used as a parameter together with the model of Prince and Blanch to simulate bubble dispersion in homogeneous regime. We_c turned out to be equal to 5. The model relies on experimental values of gas hold-up. However, a theoretical model by Kawase and Moo-Young [61] can be used for a complete theoretical formulation of the model.

Once the hydrodynamics is simulated, the paper focused on studying the effect of bubble oscillations on mass transfer looking for a theoretical explanation of the different correlations and fitting equations which try to add the effect of bubble shape on k_L.

It was found that the concentration profiles surrounding the bubbles are defined by the presence of more bubbles in the swarm, as different authors have reported. Using the theoretical value obtained by Lamont and Scott [30] for correcting k_L, the experimental values of Akita and Yoshida [17], as well as those reported by Shah et al. [1], are well predicted for sieve plates for $u_G < 0.025\ \mathrm{m\,s^{-1}}$. Bigger values of u_G are close to or in the transition regime where the bubble size distribution considered in this paper does not apply. Therefore, bubble oscillation can be considered the reason for the different correlations or adjustable parameters used so far to modify the theoretically predicted k_L.

References

[1] Y.T. Shah, B.G. Kelkar, S.P. Godbole, W.D. Deckwert, Design parameters estimations for bubble column reactor, AIChE J. 28 (1982) 353–379.
[2] N. Kantarci, F. Borak, K.O. Ulgen, Bubble column reactor, Proc. Biochem. 40 (7) (2005) 2263–2283.
[3] H.A. Jakobsen, H. Lindborg, C.A. Dorao, Modeling of bubble column reactors: progress and limitations, Ind. Eng. Chem. Res. 44 (2005) 5107–5151.

[4] P.F. Davis, A. Remuzzi, E.J. Gordon, C.F. Dewey, M.A. Gimbrone Jr., Turbulent fluid shear stresses induces vascular endothelial cell turnover in vitro, Proc. Natl. Acad. Sci. 83 (1986) 2114.
[5] J. Hua, L.E. Erickson, T.Y. Yiin, L.A. Glasgow, A review of the effects of shear and interfacial phenomena on cell viability, CRC Crit. Rev. Biotechnol. 13 (1993) 305.
[6] R. Krishna, J. Ellenberger, S.T. Sie, Reactor development for conversion of natural gas to liquid fuels: a scale-up strategy relying on hydrodynamic analogies, Chem. Eng. Sci. 51 (10) (1996) 2041–2050.
[7] Y. Pan, M.P. Duduković, M. Chang, Dynamic simulation of bubbly flow in bubble columns, Chem. Eng. Sci. 54 (13–14) (1999) 2481–2489.
[8] M.C. Ruzicka, J. Zahadnik, J. Drahoš, N.H. Thomas, Homogeneous–heterogeneous regime transition in bubble columns, Chem. Eng. Sci. 56 (2001) 4609–4626.
[9] M.C. Ruzicka, J. Drahoš, M. Fialová, N.H. Thomas, Effect of bubble column dimensions on flow regime transition, Chem. Eng. Sci. 56 (21–22) (2001) 6117–6124.
[10] M.C. Ruzicka, J. Drahoš, J.C. Mena, J.A. Teixeira, Effect of viscosity on homogeneous–heterogeneous flow regime transition in bubble columns, Chem. Eng. J. 96 (1–3) (2003) 15–22.
[11] R. Pohorecki, W. Moniuk, P. Bielski, A. Zdrójkowski, Modelling of the coalescence/redispersion processes in bubble columns, Chem. Eng. Sci. 56 (2001) 6157–6164.
[12] J.B. Joshi, Computational flow modelling and design of bubble column reactors, Chem. Eng. Sci. 56 (2001) 5893–5933.
[13] P. Chen, J. Sanyal, M.P. Duduković, Numerical simulation of bubble columns flows: effect of different breakup and coalescence closures, Chem. Eng. Sci. 60 (4) (2005) 1085–1101.
[14] M.R. Bhole, J.B. Joshi, D. Ramkrishna, Population balance modeling for bubble columns operating in the homogeneous regime, AIChE J. 53 (3) (2007) 579–588.
[15] S. Schlüter, A. Steiff, P.M. Weinspach, Modeling and simulation of bubble column reactors, Chem. Eng. Process. 31 (1992) 91–117.
[16] D. Darmana, N.G. Deen, J.A.M. Kuipers, Detailed modeling of hydrodynamics, mass transfer and chemical reactions in a bubble column using a discrete bubble model, Chem. Eng. Sci. 60 (2005) 3383–3404.
[17] K. Akita, F. Yoshida, Bubble size, interfacial area, and liquid phase mass transfer coefficients in bubble columns, Ind. Eng. Chem. Process Des. Dev. 13 (1974) 84–91.
[18] Y. Kawase, B. Halard, M. Moo-Young, Theoretical prediction of volumetric mass transfer coefficients in bubble columns for Newtonian and non-Newtonian fluids, Chem. Eng. Sci. 42 (1987) 1609–1617.
[19] R. Higbie, The rate of absorption of a pure gas into a still liquid during a short time of exposure, Trans. IChemE 31 (1935) 365–389.
[20] K. Shimizu, S. Takada, K. Minekawa, Y. Kawase, Phenomenological model for bubble column reactors: prediction of gas hold-ups and volumetric mass transfer coefficients, Chem. Eng. J. 78 (2000) 21–28.
[21] T. Wang, J. Wang, Numerical simulations of gas–liquid mass transfer in bubble columns with a CFD-PBM coupled model, Chem. Eng. Sci. 62 (24) (2007) 7107–7118.
[22] K.J. Myers, M.P. Duduković, P.A. Ramachandran, Modeling liquid phase chemical reaction and interphase mass transfer in churn turbulent bubble columns, Chem. Eng. Sci. 42 (I I) (1987) 2757–2766.
[23] R. Krishna, J.M. van Baten, Mass transfer in bubble columns, Catal. Today 79–80 (2003) 67–75.
[24] L. Han, M.H. Al-Dahhan, Gas–liquid mass transfer in a high pressure bubble column reactor with different sparger designs, Chem. Eng. Sci. 62 (2007) 131–139.
[25] H. Dhaouadi, S. Poncin, J.M. Hornut, N. Midoux, Gas–liquid mass transfer in bubble column reactor: analytical solution and experimental confirmation, Chem. Eng. Process. 47 (4) (2008) 548–556.
[26] R. Lemoine, A. Behkish, L. Sehabiague, Y.J. Heintz, R. Oukaci, B.I. Morsi, An algorithm for predicting the hydrodynamic and mass transfer parameters in bubble column an slurry bubble column reactors, Fuel Process. Technol. 89 (4) (2008) 322–343.
[27] P.H. Calderbank, M.B. Moo-Young, The continuous phase heat and mass transfer properties of dispersions, Chem. Eng. Sci. 16 (1961) 39–54.
[28] Z.G. Feng, E.E. Michaelides, Unsteady heat and mass transfer from a spheroid, AIChE J. 43 (3) (1997) 609–614.
[29] B. Haut, T. Cartageb, Mathematical modelling of gas–liquid mass transfer rate in bubble columns, Chem. Eng. Sci. 60 (22) (2005) 5937–5944.
[30] J.C. Lamont, D.S. Scott, An eddy cell model of mass transfer into surface of a turbulent liquid, AIChE J. 16 (1970) 513–519.
[31] Y. Kawase, B. Halard, M. Moo-Young, Liquid-phase mass transfer coefficients in bioreactors, Biotechnol. Bioeng. 39 (1992) 1133–1140.
[32] V. Linek, M. Kordač, M. Fujasová, T. Moucha, Gas–liquid mass transfer coefficient in stirred tanks interpreted through models of idealized eddy structure of turbulence in the bubble vicinity, Chem. Eng. Process. 43 (2004) 1511–1517.
[33] J.E. Botello-Álvarez, J.L. Navarrete-Bolaños, H. Hugo Jiménez-Islas, A. Estrada-Baltazar, R. Rico-Martínez, Improving mass transfer coefficient prediction in bubbling columns via sphericity measurements, Ind. Eng. Chem. Res. 43 (2004) 6527–6533.
[34] A.A. Kulkarni, Mass transfer in bubble column reactors: effect of bubble size distribution, Ind. Eng. Chem. Res. 46 (2007) 2205–2211.
[35] S. Nedeltchev, U. Jordan, A. Schumpe, Correction of the penetration theory based on mass-transfer data from bubble columns operated in the homogeneous regime under high pressure, Chem. Eng. Sci. 62 (2007) 6263–6273.
[36] F.J. Montes, M.A. Galán, R.L. Cerro, Mass transfer from oscillating bubbles in bioreactors, Chem. Eng. Sci. 54 (1999) 3127–3136.
[37] M.J. Prince, H.W. Blanch, Bubble coalescence and break-up in air sparged bubble columns, AIChE J. 36 (10) (1990) 1485–1499.
[38] H. Luo, H.F. Svendsen, Theoretical model for drop and bubble breakup in turbulent dispersions, AIChE J. 42 (1996) 1225–1233.
[39] J.C. Lasheras, C. Eastwood, C. Martínez-Bazán, J.L. Montañés, A review of statistical models for the break-up of an immiscible fluid immersed into a fully developed turbulent flow, Int. J. Multiphase Flow 28 (2002) 247–278.
[40] T. Wang, J. Wang, Y. Jin, Population balance model for gas–liquid flows: influence of bubble coalescence and breakup models, Ind. Eng. Chem. Res. 44 (2005) 7540–7549.
[41] M. Martín, F.J. Montes, M.A. Galán, Bubble coalescence at sieve plates. II. Effect of coalescence on mass transfer. Superficial area versus bubble oscillations, Chem. Eng. Sci. 62 (2007) 1741–1752.
[42] R.K. Sinnot, Coulson & Richardson Chemical Engineering Vol. 6: An Introduction to Chemical Engineering Design, 3ª ed., Butterworth Heinemann, Oxford, 1999.
[43] M. Martín, F.J. Montes, M.A. Galán, Numerical calculation of shapes and detachment times of bubbles generated from a sieve plate, Chem. Eng. Sci. 61 (2006) 363–369.
[44] M. Martín, F.J. Montes, M.A. Galán, Bubbling process in stirred tank reactors. I. Agitator effect on bubble size, formation and rising, Chem. Eng. Sci. 63 (12) (2008) 3212–3222.
[45] E.E. Ludwig, Applied Process Design for Chemical and Petrochemical Plants, vol. 2, Gulf Publishing Company, Houston, 1964.
[46] D.N. Miller, Scale up of agitated vessels gas liquid mass transfer, AIChE J. 20 (3) (1974) 445–453.
[47] J.F. Walter, H.W. Blanch, Bubble break-up in gas–liquid bioreactors: break-up in turbulent flow, Chem. Eng. J. 32 (1) (1986) b7–b17.
[48] R.P. Hesketh, A.W. Etchells, T.W. Russel, Bubble breakage in pipeline, Chem. Eng. Sci. 46 (1) (1991) 1–9.
[49] P.M. Wilkinson, A.V. Schayk, J.P.M. Spronken, L.L.V. Dierendonk, The influence of gas density and liquid properties on bubble breakup, Chem. Eng. Sci. 48 (7) (1993) 1213–1226.
[50] M. Martín, F.J. Montes, M.A. Galán, Influence of impeller type on the bubble break-up process in stirred tanks the effect of the impeller geometry on the break-up of bubbles, Ind. Eng. Chem. Res. 47 (16) (2008) 6251–6263.
[51] J.C. Rotta, Turbulence Stromungen, B.G. Teubner, Stuttgart, 1972.
[52] S.K. Friedlander, Smoke, Dust and Haze, Wiley, New York, 1977.
[53] C.A. Coulaloglou, L.L. Tavlarides, Description of interaction processes in agitated liquid–liquid dispersions, Chem. Eng. Sci. 32 (1977) 1289–1297.
[54] G. Marrucci, L. Nicodemo, D. Acierno, Bubble coalescence under controlled conditions, Proc. Inter. Symp. Res. Conc. Gas–Liquid Flow (1969) 95–108.
[55] J.O. Hinze, Fundamentals of the hydrodynamic: mechanism of slitting in dispersion processes, AIChE J. 1 (3) (1955) 1289–1295.
[56] F. Risso, J. Fabre, Oscillations and break-up of a bubble immersed in a turbulent field, J. Fluid Mech. 372 (1998) 323–355.
[57] C. Martínez-Bazán, J.L. Montañés, J.C. Lasheras, On the breakup of an air bubble injected into a fully developed turbulent flow. Part 1. Breakup frequency, Fluid Mech. 401 (1999) 157–182.
[58] C. Martínez-Bazán, J.L. Montañés, J.C. Lasheras, On the breakup of an air bubble injected into a fully developed turbulent flow. Part 2. Size PDF of the resulting daughter bubbles, J. Fluid Mech. 401 (1999) 183–207.
[59] G.K. Batchelor, An Introduction to Fluid Dynamics, 1ª Ed 5ª Reimp., Cambridge University press, Cambridge, 1979.
[60] C. Fleischer, S. Becker, G. Eigenberger, Detailed modeling of the chemisorption of CO_2 into NAOH in a bubble column, Chem. Eng. Sci. 51 (10) (1996) 1715–1724.
[61] Y. Kawase, M. Moo-Young, Theoretical prediction of gas hold-up in bubble columns with Newtonian and non-Newtonian fluids, Ind. Eng. Chem. Res. 26 (1987) 933–937.
[62] K. Akita, F. Yoshida, Gas hold-up and volumetric mass transfer coefficient in bubble columns, Ind. Eng. Chem. Process Des. Dev. 12 (1973) 76–80.
[63] R.R. Schroeder, R.C. Kintner, Oscillations of drops falling in a liquid field, AIChE J. (January) (1965) 5–8.
[64] A. Koynov, J.G. Khinast, G. Tryggvason, Mass transfer and chemical reactions in bubble swarms with dynamic interfaces, AIChE J. 51 (2005) 2786–2800.